



CHORUS

This is the accepted manuscript made available via CHORUS. The article has been published as:

Oxidation and crystal field effects in uranium

J. G. Tobin, S.-W. Yu, C. H. Booth, T. Tyliczszak, D. K. Shuh, G. van der Laan, D. Sokaras, D. Nordlund, T.-C. Weng, and P. S. Bagus

Phys. Rev. B **92**, 035111 — Published 6 July 2015

DOI: [10.1103/PhysRevB.92.035111](https://doi.org/10.1103/PhysRevB.92.035111)

Oxidation and Crystal Field Effects in Uranium

JG Tobin*[#], S-W Yu ,

Lawrence Livermore National Laboratory, Livermore, CA, USA,

CH Booth, T Tylizszczak, DK Shuh,

Lawrence Berkeley National Laboratory, Berkeley, CA, USA

G van der Laan,

Magnetic Spectroscopy Group, Diamond Light Source, Didcot, UK

D Sokaras, D Nordlund, T-C Weng,

Stanford Synchrotron Radiation Lightsource, Stanford, CA

and P S Bagus

Department of Chemistry, University of North Texas, Denton, TX, USA

*Corresponding Author

#email: Tobin1@LLNL.Gov

PACS numbers: 78.70.En, 71.20.Gj, 71.20.Ps, 78.70.Dm

Abstract

An extensive investigation of oxidation in uranium has been pursued. This includes the utilization of soft X-ray Absorption Spectroscopy (XAS), hard X-ray Absorption Near Edge Structure (XANES), Resonant (hard) X-ray Emission Spectroscopy (RXES), Cluster Calculations and a Branching Ratio analysis founded on Atomic Theory. The samples utilized were uranium dioxide (UO₂), uranium trioxide (UO₃) and uranium tetrafluoride (UF₄). A discussion of the role of non-spherical perturbations, i.e. crystal or ligand field effects, will be presented.

Oxidation and Crystal Field Effects in Uranium

I. Introduction

The most commonly used nuclear fuel for the generation of electricity is uranium dioxide. [1] Yet, UO_2 is not all that well understood in terms of its electronic structure. For example, there is debate whether a covalent (2) or ionic (3) picture is better. There is also substantial evidence for the apparent lack of chemical sensitivity in the soft X-ray absorption spectroscopy (XAS) measurements of uranium compounds, which has led to serious confusion concerning the nature of the electronic states. [4] Finally, in terms of the Branching Ratio Analysis of the 4d XAS of the actinides, there is the divergence that occurs in this ratio between UF_4 ($n_{5f} = 2$) and U metal ($n_{5f} = 3$), as shown in Tables 1 and 2.

The saga of the Branching Ratio Analysis utilizing the actinide 4d doublet is a tremendous success story. Well before the collection of any transuranic data, van der Laan and Thole [5] predicted the behavior of the 4d XAS of the actinides. Subsequently, these predictions were confirmed for the filling of the $5f_{5/2}$ manifold, although U metal always diverged from the intermediate curve predictions. [6,7,8] This was somewhat ironic, since the earlier data was principally that available from U materials. [9] This divergence has been explained in the past as being due to delocalization in the $5f$ states. [6,7] However, the question has magnified with the issues concerning the absence of chemical sensitivity in the XAS of uranium compounds [4], the possibility of the importance of covalency and crystal/ligand field

Oxidation and Crystal Field Effects in Uranium

effects in the 2p-5f bonds [2,4,10,11], and an experimental report that UO_2 was an $n_{5f} = 3$ material, driven by covalency effects [12]. It is these issues that will be addressed here.

II. Experimental

The soft X-ray Absorption Spectroscopy (XAS) data were collected at the Advanced Light Source at Lawrence Berkeley National Laboratory in Berkeley, CA, using the Molecular Environmental Science beamline 11.0.2 equipped with a scanning transmission X-ray microscope (STXM). [13] Soft X-ray STXM is an attractive approach for the investigation of actinides or other radioactive materials since the amount of material required is very low, offering the opportunity to investigate radioactive samples in an efficient and safe way. [14, 15] The available energy range is approximately 90–2000 eV. The materials for the STXM spectromicroscopy studies, conducted on $^{238}\text{UO}_2$ and $^{238}\text{UO}_3$, were obtained from Alfa-Aesar, Johnson Matthey. The two uranium oxide materials were finely powdered for the STXM studies. Resulting particles were transferred to 100 nm Si_3N_4 windows (Silson) by natural fibers and followed by the application of an additional Si_3N_4 window to each with epoxy, thereby forming a seal to the original window that fully encapsulated the uranium oxide. The *in-situ* phases of the two microscopic STXM samples are unknown. The STXM was used under a ~ 0.5 atm He atmosphere to record images, elemental maps, and the soft X-ray near-edge spectra XAS from suitable uranium oxide particles at the $\text{U}4d_{5/2}$ (~ 736 eV) and $\text{U}4d_{3/2}$ (~ 778 eV) edges, with a resolution better than 0.2 eV. Energy calibrations were performed at the Ne K-edge for Ne (867.3 eV). Details of the beamline characteristics can be found in Ref. 15.

Oxidation and Crystal Field Effects in Uranium

The Partial Fluorescence Yield (PFY) L_3 RXES and XANES [16,17] data were collected at SSRL wiggler beamline 6-2 using an LN_2 -cooled Si (311) double monochromator calibrated so that the inflection point of the Zr K-edge absorption from a Zr reference foil was at 17998.0 eV. The emission energy was measured using a seven-crystal Ge(777) Johann-type X-ray emission [18] spectrometer, at an emission energy of approximately 13.6 keV, corresponding to the U $L_{\alpha 1}$ edge. The energy of the emission spectrometer was calibrated by temporarily calibrating the beamline monochromator such that the first inflection point of the Au L_2 -edge absorption from a Au reference foil was at 13734.0 eV. The emission spectrometer was then calibrated to this energy by elastically scattering light from the beamline monochromator at that energy off a polycarbonate. Data were collected at room temperature (300 K). The resolution was 1.7 eV at the U $L_{\alpha 1}$ emission energy. The “regular” XANES U L_3 -edge data [19] were collected in fluorescence mode from the U L_{α} line on BL 11-2 at SSRL, with a half-tuned double Si(220) ($\theta = 0^\circ$) LN_2 -cooled monochromator on unfocused beam and a 100-element Ge solid-state detector [20], with the sample at $T = 50$ K. The effective line-width in the “regular” XANES measurements is on the order of 10 eV, much greater than the PFY XANES as reported below. Both SSRL samples were single crystals. [19] The uranium dioxide sample was part of the depleted UO_2 single crystals obtained by Los Alamos National Laboratory from Pacific Northwest National Laboratory in 1969. The uranium tetrafluoride sample was originally prepared at Y12/Oak Ridge National Laboratory.

III. Calculations

Theoretical atomic spectra were calculated in intermediate coupling using the

Oxidation and Crystal Field Effects in Uranium

well-established relativistic Hartree-Fock code of Cowan [5]. Radiative transitions were taken into account to first order. Line broadening of the photoelectron state (Lorentzian) and experimental resolution (Gaussian) were included. The Branching Ratio (BR) is defined as follows: $BR = I_{5/2}/(I_{5/2} + I_{3/2})$. I is the integrated intensity of a peak. The BR has the advantage of being intrinsically normalized, assuming that experimental conditions remain constant during the measurement of a spectrum. Further details of the calculations can be found elsewhere. [5 – 8]

For the cluster calculations, the materials models are: (1) for UO_3 an embedded octahedral UO_6 clusters with appropriate U-O bond distances and geometry for δ - UO_3 and (2) the fluorite structure of UO_2 using an embedded UO_8 cluster. [For the cluster geometries, see Ref. 21] The four-component-spinor orbitals are optimized separately for ground and core-hole configurations. Substantial covalent mixing is found between the cation $U5f$ and $U6d$ orbitals and the $O2p$ orbitals. It is inappropriate to regard the orbitals of the system as either pure cation or pure anion derived orbitals. The wave functions constructed from these optimized orbitals are mixtures of configurations. This approach is able to describe, on an equal footing, ligand field and spin-orbit splittings. In particular, we take full account of the angular momentum coupling of the open shell electrons; the system itself is able to choose the appropriate intermediate coupling between the limits of Russell-Saunders multiplets and j-j coupling. There is no adjustable parameter as in DFT+U treatments. Only dipole allowed transitions are included. More detail of the calculations will be given below; also see Ref. 22 and 23.

However, before proceeding, it is important to note the following. In the

Oxidation and Crystal Field Effects in Uranium

context of determining n_{5f} , it is necessary to take into account two different measures of the 5f occupation. One measure is the effective number of 5f electrons, which will exceed the nominal 5f occupation obtained simply by considering the oxidation state of the metal. [22] This is because of the covalent mixing of the U(5f) with ligand orbital. The other measure arises by considering the open shell character and which gives rise to the magnetic moment in many open shell compounds [24, 25]. The nominal oxidation state would be a good guide to n_{5f} for this latter measure although it would have to be modified by many-body effects that involve excitations from dominantly ligand orbitals to dominantly U(5f) orbitals. [See, for example, Ref. [26] and references therein.]

IV. Soft X-ray Absorption Spectroscopy

To begin, consider the new STXM data for UO_2 and UO_3 shown in Figure 1, along with the earlier XAS data for UF_4 and α -U from Kalkowski et al. [9] While the STXM approach has the advantage of minimizing the sample size and thus the total radioactivity of the sample, it has the corresponding drawback that the underlying spectral background can be more affected by other contributions. Thus, despite the good statistics in the peaks, there is evidence that the underlying background in the UO_2 spectrum is not always as well behaved as with macroscopic samples.

Nevertheless, it is clear that a visual examination of the four uranium spectra indicates that the spectra are almost identical, clearly without substantive change. For an example of a significant change, compare the U spectra to the Pu spectrum in the inset. While these four U 4d XAS spectra are strikingly similar, their chemical states are not. Along the side of Figure 1 is the Formal Limit of each. The Formal

Oxidation and Crystal Field Effects in Uranium

Limit is the chemical state that would occur if ionization were complete, that is, if the oxidant (O or F) succeeded in gaining complete control of the contested electrons. Of course, oxidation is rarely if ever complete and the oxidation state and ionization will include the possibility of partial oxidation and ionization. In terms of the methods of describing n_{5f} , this analysis refers to the first method described in the introduction in that it is generally considered to take into account the covalent character of the orbitals. An important exception is the semi-empirical work of Kotani and collaborators [27] where the mixing of configurations with different occupations of the metal open shell is treated. However, in this analysis, the covalent mixing of metal and ligand orbitals is not directly considered. (For example, see Ref. 26.) An example of partial ionization/oxidation is the comparison of UF_4 and UO_2 , where the formal charge is the same for both but the fluoride is considered more ionic and less covalent. The absence of any great changes between the U spectra is consistent with the results in References 4 and 9, where the 5d XAS data were shown to be essentially identical for these compounds. On the other hand, the valence band XPS spectra of these compounds are each significantly different, in a fashion that is compatible with their various Formal Limits, oxidation states and ionicities. [4]

To determine the 5f occupation of the U in the UO_2 and UO_3 , a comparison to the results of atomic calculations has been performed. This is shown in Figure 2. The calculated multiplet spectra have been convoluted with a Lorentzian ($\Gamma = 2.5$ eV) and a Gaussian ($\sigma = 0.6$ eV) line shape. The photon energy and the intensity of the calculated spectra have been normalized to the measured N_5 ($4d_{5/2}$) peak, so that the degree of agreement can be judged at the N_4 ($4d_{3/2}$) peak.

Oxidation and Crystal Field Effects in Uranium

In the top panel for Figure 2, the measured UO_2 spectrum is compared with the calculations for $5f^2$ (U^{4+}) and $5f^1$ (U^{5+}). The measurement suffers from a background problem starting from 750 eV up to and inclusive of the N_4 peak. The f^1 matches in the peak but there is a significant problem with the f^1 difference, shown in the lower part of the upper panel. It is unlikely that the background problem would abruptly stop at the beginning of the $4d_{3/2}$ peak, thus pointing toward f^2 .

Hence, this comparison suggests that f^2 is the correct configuration, but an additional analysis is required, one in which the extra background is subtracted. This operation has been performed and is shown in Figure 3, generating a BR value of 0.68, consistent with the UF_4 f^2 result. In any case, f^3 is unlikely if not impossible.

In the lower panel of Figure 2, the measured UO_3 spectrum is compared with the calculations for $5f^0$ to $5f^3$. The measured N_4 peak has a narrower line width than the N_5 , which is problematic. Usually $\text{FWHM}_{j-1/2} > \text{FWHM}_{j+1/2}$, due to increased lifetime broadening. It is worth noting that a possibly important contribution to the broadening of the N_4 and N_5 could be the unresolved multiplets arising from the coupling of the open 4d and 5f shells. [22] These issues will be discussed more below. In any case, the UO_3 does not agree with $5f^0$ (U^{6+}) but falls between $5f^1$ (U^{5+}) and $5f^2$ (U^{4+}). The fact that UO_3 is not $5f^0$ but instead between $5f^1$ and $5f^2$, is consistent with Sawatzky's suggestion that, for high oxidation states, the holes are on the oxygen atoms. [28,29,30] If this is the case, then one should be able to see these holes in the oxygen K edge XAS. In fact, the holes have been observed by Magnuson et al. [31] and others [10]. However, the number, or fractional nature, of the holes is unknown. For this reason, it is prudent

Oxidation and Crystal Field Effects in Uranium

to consider the possibility that 5f occupation is below 1, perhaps even approaching the Formal Limit of zero. Thus, the 5f occupation used here is the following:

$n_{5f}(\text{UO}_3) = 1 \pm 1$. This broad determination also permits the inclusion of other results. For example, it should be noted that a $5f^1$ initial state for UO_3 should also contribute to the XPS, but there is evidence from the XPS for a $5f^0$ initial state [21]. There is also the possibility of covalent effects in UO_3 , that may manifest themselves in the O K edge (1s) XAS [2,10,11,31].

Return now to a consideration of the peak fitting of the UO_2 STXM spectrum, as illustrated in Figure 3. After separate subtractions of linear backgrounds, each of the peaks in the UO_2 STXM spectrum has been fitted with a Lorentzian. From this we glean the following results, including proper error propagation: $\text{BR} = 0.68 \pm 0.02$, $\text{FWHM}_{3/2} = 5.40 \pm 0.08$; $\text{FWHM}_{5/2} = 6.07 \pm 0.07$. Here FWHM is the full-width at half maximum of the Lorentzian fitting function. As mentioned above, usually $\text{FWHM}_{j-1/2} > \text{FWHM}_{j+1/2}$, due to increased lifetime broadening, but here $\text{FWHM}_{j-1/2} \approx \text{FWHM}_{j+1/2}$, with very large values on the scale of 6 eV. (Note: Generally, the estimate of $\Delta\text{BR} = 0.02$ has been used on all of the BR values, such as in Tables 1 and 2.) The FWHM for the N_5 ($4d_{5/2}$) XAS peak is consistent with our cluster model calculations for UO_2 where a FWHM of 6.2 eV is found for a Voigt convolution [32] of a Gaussian (1.0 estimated for instrumental resolution) and Lorentzian (4.5 eV for lifetime broadening [33]) for each of the individual final, excited state contributions to this peak. The additional broadening of unresolved multiplets increases the effective total broadening by almost 2 eV. It may be that a differential multiplet

Oxidation and Crystal Field Effects in Uranium

broadening between the $4d_{3/2}$ and $4d_{5/2}$ XAS peaks lead to the larger FWHM for the $4d_{3/2}$ peak.

At this point, our best estimate for the 5f occupation (n_{5f}) are the following: $n_{5f}(\text{UO}_2) = 2 \pm 0.02$ and $n_{5f}(\text{UO}_3) = 1 \pm 1$, as shown in Table 2. Both of these are supported by earlier cluster calculations, with $n_{5f}(\text{UO}_2) = 2.3$ and $n_{5f}(\text{UO}_3) = 1.3$ [22]. It should be noted that, these occupations were obtained for clusters where the open shell occupation was fixed at 2 electrons for UO_2 and where UO_3 was treated as a closed shell and are based entirely on the covalent character of the orbitals. Because of the similarity of the spectra in Figure 1, we will assign $\text{BR}(\text{UO}_3) = \text{BR}(\text{UO}_2) \pm 0.02 = 0.68 \pm 0.04$. Next, an entirely independent determination of n_{5f} will be performed for UO_2 and UF_4 .

V. Hard X-ray XANES and RXES

In the recent past, a new method for the determination of 5f occupations has arisen: Resonant X-Ray Emission Spectroscopy or RXES. [16,17] It is based upon the observation that transition energies from the $2p_{3/2}$ states to the unoccupied 6d states in actinides is dependent upon the ionization and electronic configuration of the actinide [14,15,34], the development of new, high resolution hard x-ray spectrometers that permit a Partial Yield Fluorescence (PFY) data collection [16,17,18, 35] and the utilization of spectroscopic scattering techniques [16,17,35] that resemble a hard X-ray Raman experiment and lessen the lifetime broadening induced limitations of the standard approaches. [19] RXES is a two-step process involving an excitation by an incident photon of energy E_i . The electron is excited out of the initial or ground state ($U2p_{3/2}$) to a state above the Fermi level, in this

Oxidation and Crystal Field Effects in Uranium

case an unoccupied 6d state. The second step involves the decay of a 3d electron that fills the 2p hole and emits a photon with energy E_e .

A criticism of this approach has been that peak broadening can occur, which may be caused by effects in the unoccupied d density of states that are not due to intermediate valence, especially those driven by delocalization, covalency, or crystal fields. Such effects could potentially cloud or even ruin an analysis of the RXES to obtain the 5f occupancy if they are not taken into account. In fact, the UO_2 spectra in Figure 4 show exactly such broadening. It is clear that the UO_2 peaks are substantially broader than either the localized $n_{5f} = 3$ case, the UCd_{11} , or the localized $n_{5f} = 2$ case, the UF_4 .

UO_2 is considered to be a correlated-electron material and a Mott-Hubbard insulator [10], and as such, it could have an f occupancy that deviates from two and it has direct f-band involvement near the Fermi level. More importantly, the ordered cubic symmetry and octahedral coordination of the U-O nearest neighbors generates a substantial crystal field splitting of the unoccupied d states, a situation that is reduced in the more complex monoclinic structure of UF_4 . This situation is illustrated by the results in Fig. 4b of a nine atom cluster calculation of the local d density of states using FEFF 9.6.4. [19,36, 37] Three curves are shown. In each calculation, only the first shell of 8 oxygen or fluorine atoms are included along with the absorbing uranium atom. A nine atom cluster was chosen to emphasize the short-range, ligand-field nature of the e_g and t_{2g} features. The UO_2 calculation uses the nominal fluorite structure [38] and the UF_4 calculation uses the nominal monoclinic structure. [19, 39] To demonstrate the role of the fluorine atom as

Oxidation and Crystal Field Effects in Uranium

opposed to the difference in crystal structure, we also show a calculation on "UF₂", which is really the same calculation on the same structure as the UO₂ calculation, except all the oxygen atoms were replaced by fluorine atoms. In all three calculations, there is an e_g state, moving from about -7 eV in UO₂ (with respect to the vacuum energy) to about -5 eV in UF₄. The t_{2g} state is at a somewhat higher energy, all centered at about 2 eV, with the UF₄ calculation showing about a 1.5 eV split. These calculations therefore demonstrate that the e_g/t_{2g} ligand field splitting is reduced from UO₂ as one moves to the more ionic/less covalent "UF₂" compound and then further to the less symmetric UF₄ compound.

These differences can be seen in the resulting X-ray absorption calculations shown in Fig. 4(c), where we only show the calculations on the "real" UO₂ and UF₄ structures for comparison to actual data shown in Fig. 4(c). One can clearly see the effect of the larger ligand field splitting in the UO₂ calculation and the data compared to those of UF₄. There are couple of caveats here. First, there is an extra feature on the lower shoulder in the real absorption data from UF₄ near just below 17170 eV that is not reproduced in the calculation. This feature is possibly due to a direct 2p_{3/2} to 5f transition that is quadrupolar rather than dipolar in nature [16,17]. It is also possible that it is the edge jump associated with the Conduction Band Minimum (CBM) of UF₄. The increased resolution of the PFY measurement technique continues to expose spectral structure lost in earlier, lower resolution measurements. Either such feature would not be reproduced by FEFF, which does not handle the energetics of the f shells well. The second caveat is that the calculated Fermi level E_F in these small clusters is about 3 eV lower in UO₂ than the

Oxidation and Crystal Field Effects in Uranium

other calculations. This difference persists in calculations with many more atoms in the cluster, up to the largest clusters tried, of about 100 atoms. This is a common problem in FEFF, but may also be a poor reflection of the correlated electron nature of UO_2 , a quality that FEFF cannot capture. This Fermi level shift affects the photoelectron threshold energy, a shift that is not observed experimentally for UO_2 in Fig 4(c). So it should be noted that the absorption calculation in Fig. 4(c) is with respect to E_F , rather than with respect to vacuum, in order to make a direct comparison between the calculations and between the calculations and experiment. The implication of these data and calculations for the purposes of this study is that the ligand field splitting is a complicating factor in the UO_2 spectra. In contrast, UF_4 appears to be a much better, and less covalent, model for localized f^2 behavior. In fact, the ligand field splitting is even less clear in larger cluster calculations of UF_4 , creating an even sharper absorption white line. Therefore, the combination of more ionic bonding (through the replacement of oxygen with fluorine) and reduced symmetry (which further reduces the ligand field splitting) allows UF_4 to be used as a “close to ideal” localized f^2 absorption standard material.

Although FEFF does not directly treat the multiplet coupling of the open shell electrons, it may not be critically important here. The UO_2 system is a fluorite structure, with cubic symmetry for the U(IV) ion. A related, but significantly different system is $\delta\text{-UO}_3$, which has octahedral symmetry. The symmetry change is responsible for a change in the energetic order of the $6d(e_g)$ and $6d(t_{2g})$ orbitals in octahedral $\delta\text{-UO}_3$ from that in fluorite UO_2 . A closely related view of the U 6d ligand field splitting was obtained from a cluster model theoretical study of the L_3 XAS

Oxidation and Crystal Field Effects in Uranium

edge of octahedral UO_x systems, such as UO_3 , with different oxidation states. [22] In that study, the excitations from $2p_{3/2}$ to $6d(e_g)$ were shown to be ~ 7 eV above the excitations from $2p_{3/2}$ to $6d(t_{2g})$ and the $t_{2g}-e_g$ splitting was shown to be directly related to the U oxidation state and to the U-O distance. In this case, the role of the ligand field splitting for the broadening of the L_3 edge ($2p_{3/2}$) XAS peak was shown to dominate over the unresolved multiplet splittings. Interestingly, the UO_3 L_3 XANES spectrum is significantly different than that of the UO_2 L_3 XANES [9, 40]. In fact, there is a shoulder present at about 10 eV above the main white line in $\gamma\text{-UO}_3$, possibly corresponding to the 7 eV separation described above for the $\delta\text{-UO}_3$ $6d$ states. These uranium trioxide samples in Ref. 9 and 40 were $\gamma\text{-UO}_3$, a uranyl structure, not octahedral as in the $\delta\text{-UO}_3$. However, the L_3 XANES of Ba_3UO_6 , (U^{6+} , “uranate”) also has a double peak structure separated by about 10 eV.

Returning to a consideration of Figure 4(a), it is plain to see that the UO_2 peaks overlay much more with those of the UF_4 , than those of the UCd_{11} . It is also obvious that the UO_2 peaks are much broader than either of the others. The quantitative analysis is consistent with these observations. A detailed analysis of the RXES was performed using previous methods [17]. In this analysis, three peaks are used in a parametrized density of states where the peaks are held about 5 eV apart, corresponding to the difference in energy corresponding to a change of one electron in the oxydation state. This analysis produced the following results. For UF_4 : $E_{gi} = 17174.3$ eV with $\Gamma_g = 7.7$ eV; $E_{if} = 3560.4$ eV with $\Gamma_f = 3.5$ eV, $\sigma = 1.4$ eV, and $p^3 = 4\%$, $p^2 = 96\%$, and $p^1 = 0.0\%$. For UO_2 : $E_{gi} = 17173.8$ eV with $\Gamma_g = 8.1$ eV; $E_{if} = 3559.8$ eV with $\Gamma_g = 3.2$ eV; $\sigma = 2.9$ eV, and $p^3 = 2\%$, $p^2 = 98\%$, and $p^1 = 0.0\%$. Here,

Oxidation and Crystal Field Effects in Uranium

E_{gi} is the threshold photon energy, E_{if} is the transfer energy, Γ_g is the core hole broadening of the 2p core hole, Γ_f is the broadening from the 3d core hole, σ is the Gaussian width of each of the parametrized peaks in the density of states, and p^x is the relative fraction of the f^x configuration in the final state. p^n are the configuration fractions. Thus, for both UO_2 and UF_4 , $n_{5f} = 2.0$. However, the σ for the UO_2 configuration peaks is twice as large as that for the UF_4 . This broadening parallels that discussed above for the XANES in Figure 4(c) regarding CF splitting of the unoccupied 6d states. In fact, the increased width of the XES peak from UO_2 is consistent with the value of the CF splitting as obtained from optical spectroscopy of 2.8 eV [41] although a direct quantitative comparison is not possible for these data without a better understanding of the XES line shape.

Thus, the broadening in the L_3 spectra and 6d Unoccupied Density of States (UDOS) of the UO_2 relative to the UF_4 is explained as being due to the crystal/ligand field differences between the fluorite structured UO_2 and the monoclinic UF_4 . [19] The 5f occupation is determined: $n_{5f} = 2.0$ for both UO_2 and UF_4 . The $n_{5f}(UO_2)$ determination, by both 4d XAS BR and the L_3 RXES analyses, contradicts and overturns the earlier result of $n_{5f}(UO_2) = 3$ in Ref. 12.

VI. Cluster Calculations: UO_2 and UO_3

One way to address these issue of possible Crystal Field (CF) Effects is to preform BR calculations using non-spherical Hamiltonians. This is reported here for the $N_{4,5}$ (4d) XAS edges of uranium dioxide and uranium trioxide.

For XAS intensities, the many-electron dipole matrix elements from the states in the initial level to the final states have been calculated. These matrix

Oxidation and Crystal Field Effects in Uranium

elements, $ME_{ij}(\mathbf{r})$, are $ME_{ij}(\mathbf{r}) = \langle \Psi_i | \mathbf{r} | \Psi_j \rangle$, where i and j denote individual states of the initial and final level, respectively. The XAS intensity is taken to be proportional to the square, ME_{ij}^2 , where a term in the denominator is neglected, that depends on the cube of the transition energy, ΔE . Since the range of energies in the edge is ~ 20 eV and the excitation energy is almost 800 eV, it is reasonably accurate to take $(\Delta E)^3$ to be constant over this energy range. [42] In any case, the concern in XAS spectra is normally for relative intensities, $I(\text{rel})$, rather than absolute intensities.

Furthermore, sums of ME^2 over the degenerate states in the initial and final levels need to be taken to obtain the theoretical XAS spectra. We denote this matrix element as $ME_{IJ}^2(\mathbf{r}) = \sum_{ij} ME_{ij}^2(\mathbf{r})$, where the summation is taken over the degenerate states, denoted i and j , in the levels, denoted I and J . The XAS $I_{IJ}(\text{rel})$ between the I and J levels is summed over the Cartesian coordinates, $I_{IJ}(\text{rel}) = ME_{IJ}^2(x) + ME_{IJ}^2(y) + ME_{IJ}^2(z)$. The individual $I_{IJ}(\text{rel})$ are broadened by a Voigt convolution of a Lorentzian of 4.5 eV for the lifetime of the core-hole configuration and a Gaussian of 1.0 eV, as shown in Figure 5. The convoluted $I_{IJ}(\text{rel})$ are then summed to yield the full black line in Fig. 5 with underlying curves to show large individual contributions. The intensities that are shown are the relative intensities defined above scaled so that the maximum relative intensity is 0.98. The different contributions that are shown are for transitions to different final states and arise from the angular momentum coupling within and between the open shells. These states are grouped into sets of degenerate groups, commonly described as multiplets. The individual multiplets that are shown are the largest individual intensities from among a much larger set of multiplets. Two features are clear from the individual multiplets that are shown

Oxidation and Crystal Field Effects in Uranium

in Fig. 5. The first is that there is a modest multiplet splitting that contributes to the FWHM predicted for the XAS peaks. The second is that the contributions that are shown are much less than the total intensity. Thus many other individual final multiplets must contribute to the total intensity. Finally, the splittings are small enough so that they cannot be and are not resolved. The ME_{ij} are many-electron quantities and cannot be given by a single reduced matrix element between two spinors because the spinors that are used for the initial and final states are not orthogonal to each other. They involve sums and products of dipole and overlap matrix elements between the spinors optimized for the initial and final configurations. The basis sets used to describe the cation are uncontracted Gaussians. The orbitals, spinors, and wavefunctions were computed with the Dirac program system modified to interface with programs for the calculation of occupation numbers and of many-electron overlap and dipole transition matrix elements [43].

Thus, a pair of cluster calculations, for UO_2 and UO_3 , has been performed. The results are shown in Figure 5. Each of these produced a branching ratio estimate of 0.64. The Branching Ratio (BR) results are listed in Table 2 and the lower energy 5f states of the UO_2 clusters are shown in Table 3. Below, the ordering of the states in UO_2 will be discussed.

As briefly mentioned above, it is also possible to derive 5f occupations from such cluster calculations. For uranium dioxide and uranium trioxide, these results have been published earlier [Table 5 of Ref. 23], with the result being $n_{5f}(UO_2) = 2.33$ and $n_{5f}(UO_3) = 1.32$. However, this raises an interesting question concerning

Oxidation and Crystal Field Effects in Uranium

the definition of 5f occupancy and by extension the occupations of other "unfilled" or "partly" filled shells.

One meaning is the fractional number of electrons that occupy a shell because there is covalent mixing of the metal orbitals with the ligand orbitals. In particular, some of the closed shell dominantly ligand orbitals are bonding combinations of metal and ligand orbitals. The reason for this qualification is that the mixing depends on the point group symmetry of the orbitals and their spatial orientation. Further, some of the open shell, dominantly metal cation orbitals form anti-bonding combinations with the ligand orbitals. The occupations or populations of the 5f in these covalent orbitals can be estimated in several ways ranging from a Mulliken population analysis [44-46], which has its limitations, to a projection of atomic orbitals on the oxide orbitals, which is the preferred method of the authors of Ref. 23. In that paper, it is shown how a projection can be used to give unique estimates of the uncertainties of the assignments of charge and the assignments of n_{5f} .

A couple of comments on this definition need to be made. It leads to an increase in the open shell occupation over the nominal value given by assuming that the open shell is a pure cation without any covalent mixing. This is because the closed shell orbitals lead to an increase of n_{5f} that is multiplied by the occupation of these orbitals, which are filled shells. The open shell orbitals, having partly ligand character, contribute to n_{5f} less than would be expected from their occupation because they are not pure cation orbitals. However, the increase in the contribution to n_{5f} from the closed-shell dominantly-ligand orbitals is larger than the loss from

Oxidation and Crystal Field Effects in Uranium

the fractionally occupied "open shell" orbitals. Hence the occupation of the open shell n_{5f} , or n_{3d} for 3d transition metal compounds, is larger than found from the nominal oxidation state. This definition is more important for some properties than for others. For example, it is very important for the "crystal field" splitting because there is differential covalency among the orbitals of the open shell; e.g., the energy splitting of the different 5f spinors. It can also be seen in the much larger splittings of the different 6d orbitals, where it has been shown that the covalent mixing is larger than in the 5f shell orbitals. [22] The level of importance of covalent mixing for 5f structures in XPS and XAS may be less but it may not be negligible. One of the ways that the covalent mixing can affect the XPS and XAS is that the loss of metal character will modify, probably reduce, the multiplet splittings. However, due to the large lifetime broadening in the 4d XAS, these changes in multiplet structure may be lost.

The other definition of occupation comes from the open shell configuration, usually equivalent to the oxidation state and is usually an integer. It is exactly an integer unless one considers many-body effects where there is a mixing of configurations where the open shell occupation is changed. One way to make this familiar is with the Charge Transfer from ligand to metal that is used to explain satellites in XPS that was originally proposed by Sawatzky [28,29,30].

An alternative to this conceptual framework would be to describe the configuration mixing as involving configurations where bonding electrons are excited to anti-bonding shells. In some measure, these two descriptions are related and use different words for similar many-body effects. However, it may be that the

Oxidation and Crystal Field Effects in Uranium

bonding to anti-bonding excitation provides a better focus on the essential physics than the charge transfer terminology. These two descriptions were discussed in a recent publication. [26] However, as far as the atomic model analysis of XAS is concerned, such many body effects are not included. Thus, the main effect of covalency will come in how the changes it causes in the exchange and Coulomb integrals will affect the angular momentum coupling of the excited XAS states and, as a consequence, their energies and their degree of intermediate coupling. This effect may manifest itself in the different scaling factors for the atomic two electron integrals. However from this definition, n_{5f} for UO_3 must be zero since UO_3 is a closed shell system.

Finally, this section is closed by returning to the issue that the cluster wavefunctions that were described earlier in this section only include determinants that allow the correct angular momentum coupling within the open shells. They do not include determinants that would represent the kind of Charge Transfer described in the preceding paragraph. Thus for the XAS, our wavefunctions do not include this particular many-body effect. For the final states of XPS transitions of Ref. 21, such configurations must and have been included, using the formalism of shake configurations in order to describe the XPS satellites. The choice of the terminology shake is to describe the excitation of filled bonding levels into unfilled or partially filled anti-bonding levels; the differentiation of bonding and anti-bonding levels is considered further in the next section where we discuss covalency in more detail. However, our treatments of XAS and XPS [26] do not include the shake, or charge transfer configurations for the ground initial state. By comparing with the results of

Oxidation and Crystal Field Effects in Uranium

other spectroscopies, there is evidence that the neglect of shake configurations for the ground state, where the core levels are filled, is a good approximation. For UO_2 , the magnetic moment determined for the ground state of the UO_8 cluster is $1.92 \mu_B$. This is in reasonably good agreement with the experimental value of $1.74 \mu_B$ [47,48]. It is especially impressive, considering that it is difficult to determine this property with rigorous electronic structure methods. For example, DFT + U calculations give the magnetic moment to be $2.1\text{-}2.2 \mu_B$ [49]. This result for μ_B suggests that the departures of n_{5f} from 2 arise from covalent mixing rather than from excitations, or “charge transfer” into the open 5f shell. For UO_3 , we have been able to accurately describe the 4f XPS satellites using a single closed shell determinant to describe the initial state [21]. This is an indication that the departure of n_{5f} from 0 arises from the covalent mixing of U(5f) with O orbitals. The apparent inconsistency between the XAS and the XPS analysis for n_{5f} is a question that needs to be resolved.

VII. Crystal Field Effects and Covalence

In this section, several key aspects of crystal field effects and covalence in oxidized uranium will be discussed.

First, it is of importance to remember that there is clear experimental evidence for the direct overlap of U5f-O2p and U6d-O2p states in the UDOS of UO_2 , using soft X-ray XAS, Bremsstrahlung Isochromat Spectroscopy and Resonant Inverse Photoelectron Spectroscopy [10,11]. The question arises: is it possible to connect that data with the L_3 data reported here? To do that, a comparison of spectra and UDOS is performed in Figure 6. In Figure 6, the results of cluster calculations by Ryzhkov et al., for UF_4 and UO_2 , will be used [50,51]. The

Oxidation and Crystal Field Effects in Uranium

advantages of using Ryzhkov's calculations are threefold: (1) Ryzhkov's calculations pre-dated this work by several years; (2) they demonstrate the generality of the results; and (3) Ryzhkov's results were obtained using the same methodology for both systems.

In the region of the absorption edge, it is possible to observe the large spectral features known as XANES (Figures 4 and 6). For the U L₃ (2p_{3/2}) edge, the threshold is near 17,160 eV. The experimental spectra in Figure 4 for UO₂ and UF₄ duplicate the earlier results of Kalkowski et al. for both compounds [9], but with much better resolution, owing to the PFY detection scheme. In general, XANES gives a measure of the unoccupied density of states [36]. This is confirmed in Figure 6, by comparing the experimental XANES spectra with simulated spectra, using the 6d state distributions calculated in Ryzhkov's cluster models for UO₂ and UF₄ [50,51]. Here, Doniach-Sunjic lineshapes [52] have been used, with the asymmetry parameter (α) of 0.3 and a series of values for the lifetime width (Γ), with $\Gamma = 1/2$ the Full Width at Half Maximum (FWHM) of the Lorentzian component. The underlying assumption is that each state generates a contribution of equal intensity. As can be seen, there is a good agreement between the experimental and simulated spectra, particularly if the UO₂ state distribution is adjusted slightly to optimize agreement with the soft X-ray N₇ (4d_{7/2}) spectrum from Reference 10. Then the agreement for the L₃ PFY XANES with the $\Gamma = 2$ eV and the "regular" L₃ PFY XANES with the $\Gamma = 4$ eV [17] is clearly evident. It should be noted that although the energy broadening determination from the UF₄ edge jump indicates that the L₃ PFY XANES comparison should be made at $\Gamma = 2$, the match may be even better at $\Gamma = 3$ eV. As

Oxidation and Crystal Field Effects in Uranium

always, experimental spectra are never as sharp as theoretical spectra. Thus, the broadening of the L_3 PFY for UO_2 is clearly consistent with the earlier, higher resolution XAS that demonstrated the $U6d-O2p$ overlap and the narrowing of the $UF_4 L_3$ versus the UO_2 is consistent with the reduced symmetry of the structure of UF_4 versus that of UO_2 . Plus, once again, it is noted that the Ryzhkov calculations pre-date this work by several years and the L_3 data address the $U6d-O2p/F2p$ hybridization.

Now, consider the impact of crystal field (CF) splitting upon the $U5f$ BR calculations. It is possible to include CF effects in a full and equal way with spin-orbit in the atomic calculations based upon Cowan's code [53,54]. However, the values of the crystal field parameters are often not very well known from experiment. Here, these calculations have been performed, utilizing the experimental CF parameters from Amoretti et al. [47,48] for UO_2 . In an attempt to provide a general result, not just that for UO_2 with $n_{5f} = 2$, the CF parameters for uranium dioxide were applied across the series of $n_{5f} = 1$ to 4, i.e. up through Np. The CF results in Table 4 were then couched as a percentage deviation from the purely spherical intermediate results (Table 1). These calculations were performed with full matrix diagonalization in intermediate coupling with CF. As can be seen in Table 4, the effect upon the BR is very small and completely negligible.

Furthermore the interpretation, of Amoretti et al [47,48] for UO_2 , is supported by the cluster calculations performed in this work. This can be seen in Table 3. Here the energies of the f^2 states and their symmetries are listed. The cluster calculations have the same ground state Γ_5 , but the order of the higher

Oxidation and Crystal Field Effects in Uranium

energy excited levels is different, which may depend on the tuning of the V_6 with respect to the V_4 parameter. However, note that the four lowest levels are all split off from the $J=4$ level (in the limit of small CF), suggesting that their XAS branching ratio would be very similar. Because of the broadening in the 4d XAS spectra, the possible differences in the higher energy fine structure are lost. Perhaps other variants of higher resolution spectroscopy, such as RIXS [55, 56], could resolve this fine structure. However, 4d XAS, with the averaging imposed by the lifetime broadening, will not resolve these differences and the BR analyses will follow the atomic model results without the need for the inclusion of CF effects. In essence, while the BR ratio analysis can provide information concerning the occupation of the 5f levels in localized actinide systems, it is blind to crystal field effects.

It may be that this trend is universal for the actinides. For lower Z cases, such as U materials, this is caused by the effect of the 5f crystal field upon the low lying 5f states being smaller than that of the 5f spin-orbit interaction and the 5f Coulomb interaction, as described above. For the higher Z actinides such as Pu, the 5f levels collapse inward and are insensitive to the crystal field: e.g. monoclinic α -Pu and fcc δ -Pu have the same BR value. [57] The rule for small perturbations is derived in Sec. V of Ref. 5. It appears that BR only measures the spin-orbit interaction of the 5f, and it clearly seems the CF is not as important for the U5f states as for the U6d states. The CF is important in the 6d states, but this has no influence on the $N_{4,5}$ (4d) BR. In localized materials the $N_{4,5}$ (4d) BR is very close to the intermediate coupling value. In a delocalized material the BR reduces towards the

Oxidation and Crystal Field Effects in Uranium

LS coupling limit [6,7]. The CF as a point charge model does not lead to delocalization, it merely changes a sphere in a cube.

Finally, all of the BR results are summarized in Figure 7. The dynamic range of the Branching Ratio analysis is inside two boundaries: The statistical value of 0.6 (throughout) and the jj limit curve (solid gray line), running from 0.6 to 1.0. The solid black line is the intermediate model result, also shown in Figure 1. The experimental results, shown typically with error bars of +/- 0.02, are from XAS (filled red diamonds), EELS (hollow blue squares) and UO₂-STXM and UO₃-STXM (both- filled orange circle with error bars). There are also new results from cluster calculations for UO₂ and UO₃ (both-filled green circle with error bars). The UO₂-STXM and UF₄-XAS results overlap perfectly, both at $n_{5f} = 2$. The dashed red curve connects the experimental results and the assumed statistical value of 0.6 at $n_{5f} = 0$. The experimental divergence at U ($n_{5f} = 3$) remains. For localized systems, the intermediate coupling theory remains an excellent line of calibration. The problem arises with the horizontal region near BR = 0.68. For uranium compounds, intermetallics and alloys, without prior knowledge of the oxidation state/ionization, it is unclear where to sit on the horizontal line between $2 \leq n_{5f} \leq 3$ and perhaps even $0 \leq n_{5f} \leq 3$, if the UO₃-STXM result is included

VIII. Conclusions

1. The hypothesis in Ref. 4 of the potential importance of CF effects in the BR ratio analysis of 5f states was incorrect.
2. Both UO₂ and UF₄ are $n_{5f}=2$ materials. The combination of the 4d XAS BR and RXES analyses is particularly powerful. The effect of CF in the L₃

Oxidation and Crystal Field Effects in Uranium

XANES spectrum and U6d states of the UO_2 is obvious and strong.

3. CF broadening in the L_3 RXES spectroscopy does not preclude a successful analysis.
4. The prior experimental result that $n_{5f}(\text{UO}_2) = 3$ and the proposed causation by covalent bonding was incorrect. UO_2 is an $n_{5f}=2$ material and analysis within a simple, ionically localized picture provides the correct result.
5. UO_3 appears to be an $n_{5f} = 1$ material. The XPS measurements of UO_3 are consistent with a closed shell electronic structure [21] where, however, there is substantial covalent mixing of U(5f) with O(2p). [23] On the other hand, the 4d XAS points toward an open shell structure where $n_{5f}=1$.
6. While the 4d XAS BR analysis is blind to CF effects, crystal field and covalence remain important. This is manifested in the reordering of the excited states in uranium dioxide cluster calculations and past XAS and RIPES studies. It also presents an opportunity for further studies of actinide materials by complementary and high resolution methods such as RIXS, to fully unravel the characteristics of bonding in actinide materials.
7. For localized actinide systems, the 4d XAS BR analysis founded upon the utilization of the intermediate coupling scheme remains a powerful tool.
8. For delocalized actinide systems, the BR analysis is problematic. In particular for uranium compounds and intermetallics of unknown oxidation state/ionization, the horizontal section of the experimental

Oxidation and Crystal Field Effects in Uranium

curve in Figure 7 places a fundamental limitation upon the analysis:
unless the oxidation state/ionization is independently determined, a BR
value of or near 0.68 means that the n_{5f} could vary between 2 and 3,
possibly 0 and 3.

Oxidation and Crystal Field Effects in Uranium

IX. Acknowledgements

Lawrence Livermore National Laboratory is operated by Lawrence Livermore National Security, LLC, for the U.S. Department of Energy, National Nuclear Security Administration under Contract DE-AC52-07NA27344. Work at Lawrence Berkeley National Laboratory (CHB, DKS) was supported by the Director, Office of Science, Office of Basic Energy Sciences (OBES), Division of Chemical Sciences, Geosciences, and Biosciences (CSGB), Heavy Element Chemistry (HEC) Program of the U.S. Department of Energy under Contract No. DE-AC02-05CH11231. The XANES and RXES data were collected at BL-6-2 and BL-11-2 at SSRL. The ALS and TT are supported by the Director, Office of Science, OBES of the U.S. Department of Energy at LBNL under Contract No. DE-AC02-05CH11231. MES Beamline 11.0.2 is supported by the Director, Office of Science, OBES, CSGB Condensed Phase and Interfacial Molecular Sciences and HEC programs, both of the U.S. Department of Energy at LBNL under Contract No. DE-AC02-05CH11231. PSB acknowledges support by the Geosciences Research Program, Office of Basic Energy Sciences, U.S. DOE; the support for PSB is through Grant No. DE-FG02-04ER15508. The Stanford Synchrotron Radiation Lightsource is a national user facility operated by Stanford University on behalf of the DOE, Office of Basic Energy Sciences. The UF_4 sample was originally prepared at Oak Ridge National Laboratory and provided to LLNL by J. S. Morrell of Y12. [4] JGT wishes to thank (1) Glenn Fox and the PRT Program at LLNL for support during his sabbatical at LBNL; (2) DKS for his hosting of the sabbatical at GTSC/LBNL; and (3) CHB for the opportunity to learn new hard X-ray skills and collect data in the middle of the night again. We thank Eric D. Bauer and Mark T. Paffett of LANL for making the UO_2 sample available to us and we thank Wayne Lukens for many enlightening discussions about crystal field theory.

Oxidation and Crystal Field Effects in Uranium

X. References

1. S.-W. Yu and J.G. Tobin, *J. Electron Spectroscopy Rel. Phen.* **187**, 15 (2012) and references therein.
2. I.D. Prodan, G.E. Scuseria, R.L. Martin, *Phys. Rev. B* **76**, 033101 (2007).
3. L. Petit, et al., *Phys. Rev. B* **81** 045108 (2010).
4. J. Tobin, *J. Electron Spectroscopy Rel. Phen.* **194**, 14 (2014).
5. G. van der Laan and B.T. Thole, *Phys. Rev. B* **53**, 14458 (1996).
6. G. van der Laan, K.T. Moore, J.G. Tobin, B.W. Chung, M. A.Wall, and A. J. Schwartz, *Phys. Rev. Lett.* **93**, 097401 (2004).
7. J. G. Tobin, K. T. Moore, B. W. Chung, M. A. Wall, A. J. Schwartz, G. van der Laan, and A. L. Kutepov, *Phys. Rev. B* **72**, 085109 (2005).
8. K. T. Moore, G. van der Laan, M. A. Wall, A. J. Schwartz, and R. G. Haire, *Phys. Rev. B* **76**, 073105 (2007).
9. G. Kalkowski, G. Kaindl, W.D. Brewer and W. Krone, *Phys. Rev B* **35**, 2667 (1987).
10. S.-W. Yu, J. G. Tobin, J. C. Crowhurst, S. Sharma, J. K. Dewhurst, P. Olalde-Velasco, W. L. Yang, and W. J. Siekhaus, *Phys. Rev. B* **83**, 165102 (2011).
11. J.G. Tobin and S.-W. Yu, *Phys. Rev. Lett.* **107**, 167406 (2011).
12. K. T. Moore, G. van der Laan, R. G. Haire, M. A. Wall, and A. J. Schwartz, *Phys. Rev. B* **73**, 033109 (2006).
13. H. J. Nilsson, T. Tylliszczak, R. E. Wilson, L. Werme and D. K. Shuh, *Anal. Bioanal. Chem.* **383**, 41 (2005).
14. X.-D. Wen, M. W. Löble, E. R. Batista, Eve Bauer, K. S. Boland, Anthony K. Burrell, S. D. Conradson, S. R. Daly, S. A. Kozimor, S. G. Minasian, R. L. Martin, T. M. McCleskey, B. L. Scott, D. K. Shuh, T. Tylliszczak, *J. Electron Spectroscopy and Rel. Phen.* **194** 81 (2014).
15. H. Bluhm, K. Andersson, T. Araki, K. Benzerara, G. E. Brown, Jr., J. J. Dynes, S. Ghosal, H.-Ch. Hansen, J. C. Hemminger, A. P. Hitchcock, G. Ketteler, E. Kneidler, J. R. Lawrence, G. G. Leppard, J. Majzlam, B. S. Mun, S. C. B. Myneni, A. Nilsson, H. Ogasawara, D. F. Ogletree, K. Pecher, D. K. Shuh, M. Salmeron, B.

Oxidation and Crystal Field Effects in Uranium

- Tonner, T. Tyliczszak, and T. H. Yoon, "Soft X-ray Microscopy and Spectroscopy at the Molecular Environmental Science Beamline of the Advanced Light Source," *J. Electron Spectros. Rel. Phenom.* **150**, 86-104 (2006).
16. C.H. Booth, Yu Jiang, D.L. Wang, J.N. Mitchell, P.H. Tobash, E.D. Bauer, M.A. Wall, P.G. Allen, D. Sokaras, D. Nordlund, T.-C. Weng, M.A. Torrez, and J.L. Sarrao, *Proc. Natl. Acad. Sci.* **109**, 10205 (2012).
 17. C.H. Booth, S.A. Medling, Y. Jiang, E.D. Bauer, P.H. Tobash, J.N. Mitchell, D.K. Veirs, M.A. Wall, P.G. Allen, J.J. Kas, D. Sokaras, D. Nordlund, T.-C. Weng, *J. Electron Spectroscopy and Rel. Phen.* **194** 57 (2014).
 18. D. Sokaras, T.-C. Weng, D. Nordlund, R. Alonso-Mori, P. Velikov, D. Wenger, A. Garachtchenko, M. George, V. Borzenets, B. Johnson, T. Rabedeau and U. Bergmann, *Rev. Sci. Instrum.* **84**, 053102 (2013).
 19. J.G Tobin, C.H. Booth, W. Siekhaus and D.K. Shuh, "EXAFS Investigation of UF₄," *J. Vac. Sci. Tech. A* **33**, xxxx, (2015) and references therein.
 20. J. J. Bucher, P. G. Allen, N. M. Edelstein, D. K. Shuh, N. W. Madden, C. Cork, P. Luke, D. Pehl, and D. Malone, *Review of Scientific Instruments* **67**, 3361 (1996).
 21. P.S. Bagus, C.J. Nelin and E.S. Ilton, *J. Chem. Phys.* **139**, 244704 (2013).
 22. C.J. Nelin, P. S. Bagus and E. S. Ilton, *RSC Advances* **4**, 7148 (2014).
 23. P. S. Bagus and C. J. Nelin, *J. Electron Spectroscopy Rel. Phen* **194**, 37 (2014).
 24. P. S. Bagus, E. S. Ilton, R. L. Martin, H. J. A. Jensen, S. Knecht, *Chem. Phys. Lett.* **546**, 58 (2012).
 25. H. U. Rahman and W.A. Runciman, *J. Phys. Chem. Solids* **27**, 1833 (1966).
 26. P. S. Bagus, E. S. Ilton, C. J. Nelin, *Surface Science Report* **68**, 273 (2013).
 27. A. Kotani and T. Yamazaki, *Prog. Theor. Phys. Supplement* **108**, 117 (1992).
 28. G.A. Sawatzky, Max Planck/U. British Columbia-Vancouver Center for Quantum Materials, <http://conservancy.umn.edu/handle/11299/163182>)
 29. G. van der Laan, C. Westra, C. Haas, and G. A. Sawatzky, *Phys. Rev. B* **23**, 4369 (1981).
 30. J. Zaanen, C. Westra, and G. A. Sawatzky, *Phys. Rev. B* **33**, 8060 (1986).

Oxidation and Crystal Field Effects in Uranium

31. M. Magnuson, S.M. Butorin, L. Werme, J. Nordgren, K.E. Ivanov, J.-H. Guo, D.K. Shuh, *Applied Surface Science* **252**, 5615 (2006).
32. J. A. Gubner, *J Phys. A* **27**, L745 (1994).
33. J. L. Campbell and T. Papp, *Atomic Data and Nuclear Data Tables* **77**, 1–56 (2001).
34. S. D. Conradson, B. D. Begg, D. L. Clark, C. Den Auwer, F. J. Espinosa-Faller, P. L. Gordon, N. J. Hess, R. Hess, D. W. Keogh, L. A. Morales, M. P. Neu, W. Runde, C. D. Tait, D. K. Veirs, and P. M. Vilella, *Inorg. Chem.* **42**, 3715 (2003).
35. K. Hamalainen, D. P. Siddons, J. B. Hastings and L. E. Berman, *Phys. Rev. Lett.* **67**, 2850 (1991).
36. B.K. Teo, "EXAFS Basic Principles and Data Analysis," Springer Verlag, New York, 1986.
37. J.J. Rehr, J.J. Kas, F.D. Vila, M.P. Prange, K. Jorissen, *Phys. Chem. Chem. Phys.* **12** 5503 (2010).
38. R. W. G. Wyckoff, "Crystal Structures", Interscience Publishers, New York, 2nd ed., 1964.
39. R. B. Roof, and D. T. Cromer, *Acta. Cryst.* **17**, 555 (1964).
40. S. Van den Berghe, M. Verwerft, J.-P. Laval, B. Gaudreau, P. G. Allen, A. Van Wyngarden, *J. Solid State Chem.* **166**, 320 (2002).
41. J. Schoenes, *J. Chem. Soc. Faraday Trans.* **2**, 83, 1205 (1987).
42. H. A. Bethe and E. W. Salpeter, *Quantum Mechanics of One- and Two-Electron Atoms*, Academic Press, 1957.
43. DIRAC, a relativistic ab initio electronic structure program, Release DIRAC08 (2008), written by L. Visscher, H. J. Aa. Jensen, and T. Saue, with new contributions from R. Bast, S. Dubillard, K. G. Dyall, U. Ekström, E. Eliav, T. Fleig, A. S. P. Gomes, T. U. Helgaker, J. Henriksson, M. Iliaš, Ch. R. Jacob, S. Knecht, P. Norman, J. Olsen, M. Pernpointner, K. Ruud, P. Sałek, and J. Sikkema, <http://dirac.chem.sdu.dk>.
44. C. W. Bauschlicher and P. S. Bagus, *J. Chem. Phys.*, **81**, 5889 (1984).

Oxidation and Crystal Field Effects in Uranium

45. M.V. Ryzhkov, A. Mirmelstein, S.-W. Yu, B.W. Chung and J.G. Tobin, *Intl. J. Quantum Chem.* **113**, 1957 (2013).
46. M.V. Ryzhkov, A. Mirmelstein, B. Delley, S.-W. Yu, B.W. Chung, J.G. Tobin, "The Effects of Mesoscale Confinement in Pu Clusters," *J. Electron Spectroscopy and Rel. Phen.*, **194**, 45 (2014); <http://dx.doi.org/10.1016/j.elspec.2013.11.015>.
47. G. Amoretti, A. Blaise, R. Caciuffo, J. M. Fournier, M. T. Hutchings, R. Osborn and A. D. Taylor, *Phys. Rev. B* **40**, 1856 (1989).
48. N. Magnani, P. Santini, G. Amoretti, and R. Caciuffo, *Phys. Rev. B* **71**, 054405 (2005).
49. F. Zhou and V. Ozolins, *Phys. Rev. B* **83**, 085106 (2011).
50. Yu. A. Teterin, K. I. Maslakov, M. V. Ryzhkov, O.P. Traparic, L. Vukcevic, A. Yu. Teterin, and A. D. Panov, *Radiochemistry* **47**, 215 (2005).
51. A. Yu. Teterin, Yu. A. Teterin, K. I. Maslakov, A. D. Panov, M. V. Ryzhkov, L. Vukcevic, *Phys. Rev. B* **74**, 045101 (2006).
52. J.G. Tobin and F.O. Schumann, *Surface Science* **478**, 211 (2001).
53. G. van der Laan and B.T. Thole, *Phys. Rev. B* **43**, 13401 (1991).
54. B.T. Thole, G. van der Laan and P.H. Butler, *Chem. Phys. Lett.* **149**, 295 (1988).
55. K.O. Kvashnina, S.M. Butorin, P. Martin and P. Glatzel, *Phys. Rev. Lett.* **111**, 253002 (2013).
56. T. Vitova, K. O. Kvashnina, G. Nocton, G. Sukharina, M. A. Denecke, S. M. Butorin, M. Mazzanti, R. Caciuffo, A. Soldatov, T. Behrends, and H. Geckeis *Phys. Rev. B* **82**, 235118 (2010).
57. J.G. Tobin, P. Söderlind, A. Landa, K.T. Moore, A.J. Schwartz, B.W. Chung, M.A. Wall, J.M. Wills, R.G. Haire, and A.L. Kutepov, *J. Phys. Cond. Matter* **20**, 125204 (2008).

Oxidation and Crystal Field Effects in Uranium

Table 1

Comparison of Some Different Coupling Schemes for the Branching Ratios

n	jj Limit [7]	Intermediate Coupling [6,7,8]
0	0.60	0.59
1	0.64	0.63
2	0.69	0.68
3	0.75	0.72
4	0.81	0.76
5	0.90	0.82
6	1.00	0.93

Oxidation and Crystal Field Effects in Uranium

Table 2

Source	n_{5f}	BR	Ref.
UF ₄ -XAS	2	0.68	6, 7, 9
U-XAS	3	0.68	6, 7, 9
Pu-XAS	5	0.81	6, 7
Th-EELS	1	0.65	6, 7, 8
U-EELS	3	0.69	6, 7, 8
Np-EELS	4	0.74	8
Pu-EELS	5	0.83	6, 7, 8
Am-EELS	6	0.93	8
UO ₂ -STXM	2	0.68	This work
UO ₃ -STXM	1 +/- 1	0.68	This work
UO ₂ -Cluster	2 +/- 0.3	0.64	This work and Ref. 23.
UO ₃ -Cluster	1 +/- 0.3	0.64	This work and Ref. 23.

Oxidation and Crystal Field Effects in Uranium

Table 3

Amoretti et al. [47]		UO ₈ Cluster	
LIR	RE(meV)	LIR	RE(meV)
$\Gamma_5 = T_2$	0	$\Gamma_5 = T_2$	0
$\Gamma_3 = E$	150.1	$\Gamma_1 = A_1$	152
$\Gamma_4 = T_1$	166.7	$\Gamma_4 = T_1$	159
$\Gamma_1 = A_1$	174.8	$\Gamma_3 = E$	186
$\Gamma_5 = T_2$	652	$\Gamma_3 = E$	659

LIR: Level Irreducible Representation

RE: Relative Energy (meV)

Oxidation and Crystal Field Effects in Uranium

Table 4

Atomic Model BR Calculations including Crystal Field

$$\text{Reduction factor} = \frac{[(\text{BR without CF}) - (\text{BR with CF})]}{(\text{BR without CF})}$$

Configuration	Reduction Factor
f ⁰	0
f ¹	0.00003
f ²	0.0005
f ³	0.0007
f ⁴	0.004

Oxidation and Crystal Field Effects in Uranium

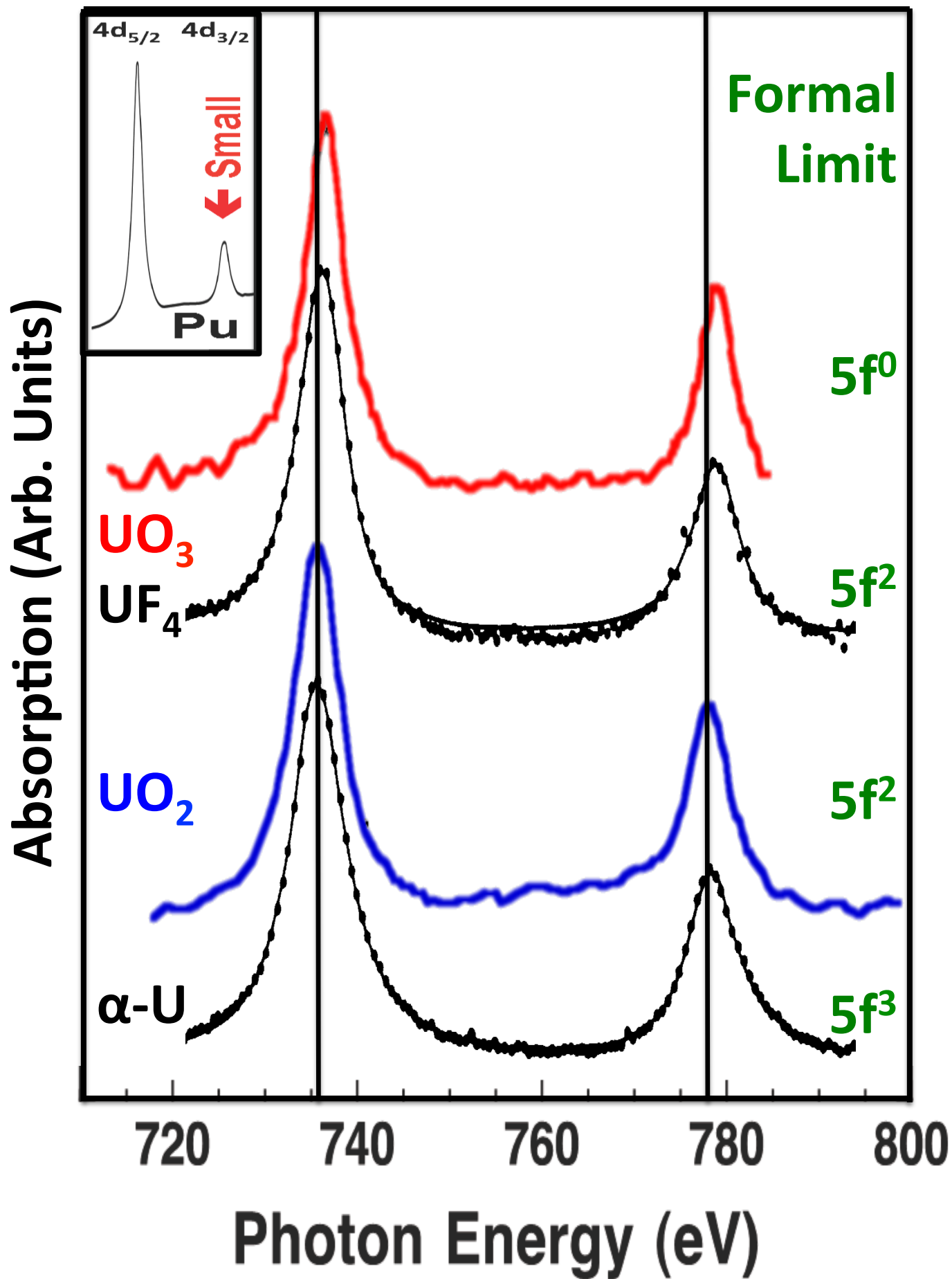
Figure Captions

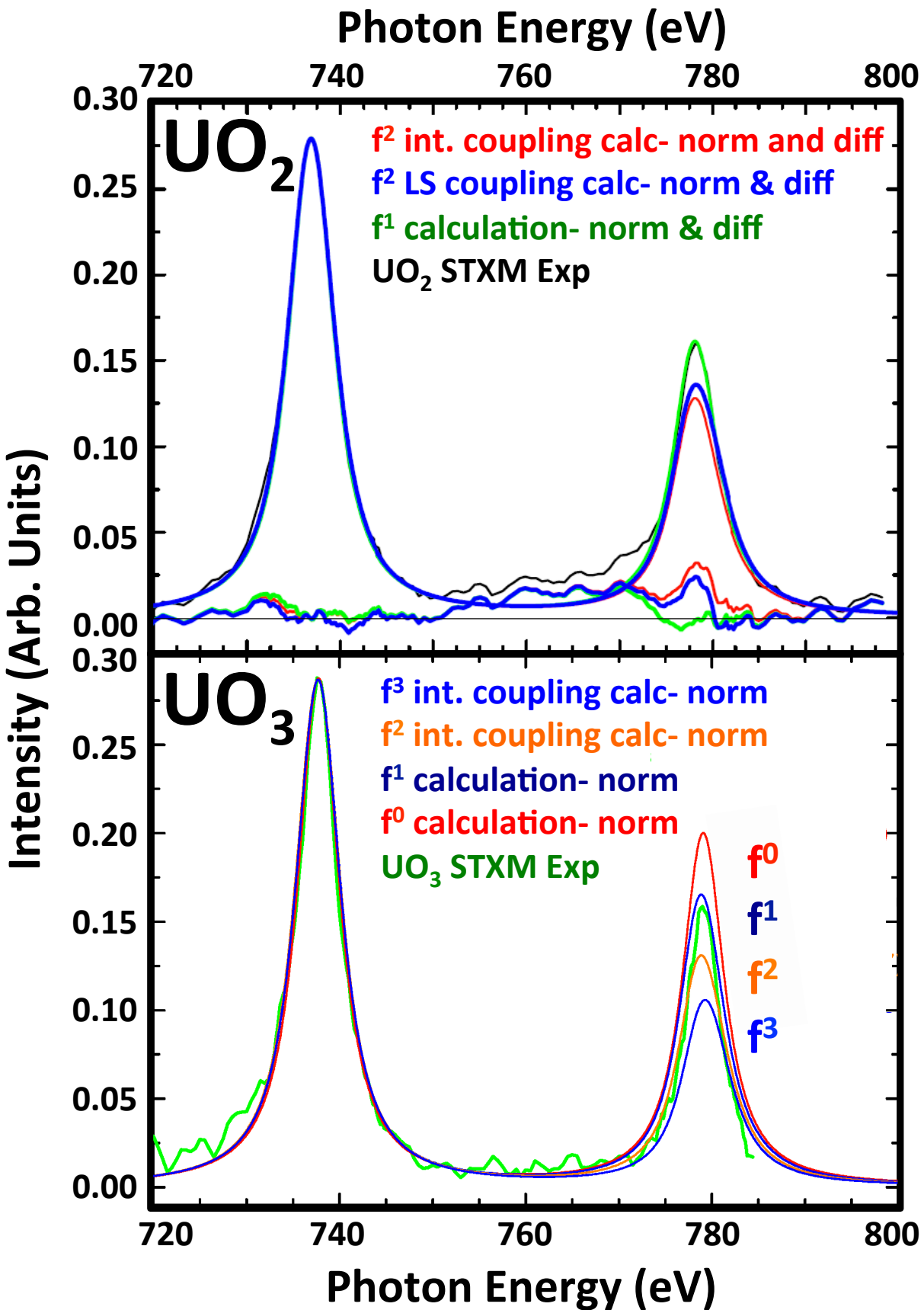
- Figure 1 X-ray Absorption Spectroscopy data of the $4d_{5/2}$ (near 736 eV) and $4d_{3/2}$ (near 778 eV) peaks of α -U (black), UO_2 (blue), UF_4 (black) and UO_3 (red) are shown here. The U and UF_4 spectra are from Reference 9. The UO_2 and UO_3 data are from microscopic samples used at the Advanced Light Source. While UO_2 and UF_4 have the same formal charge limit, it is expected that their oxidation states/ionizations are different, with UF_4 being more ionic and less covalent in nature. The inset shows the corresponding peaks for Pu [6,7].
- Figure 2 Here is shown an analysis of the STXM spectra for UO_2 and UO_3 , by comparison to the calculated atomic spectra for various n_{5f} values and coupling schemes. Top Panel: UO_2 experiment (black); f^1 (green), f^2 LS coupling (blue); and f^2 intermediate coupling (red). Bottom Panel: UO_3 experiment (green); f^0 (red); f^1 (dark blue); f^2 intermediate coupling (orange); f^3 intermediate coupling (blue).
- Figure 3 After separate subtractions of linear backgrounds, each of the peaks in the UO_2 STXM spectrum has been fitted with a Lorentzian. The data is shown as orange squares. The fitted Lorentzians are green lines.
- Figure 4 Shown here are: (a) the Partial Fluorescence Yield (PFY) results for the L_3 Resonant X-ray Emission Spectroscopy (RXES) and (b) the FEFF calculations of the 6d density of states; (c) the PFY results for the L_3 X-ray Absorption Near Edge Structure (XANES) measurements. 4(a): UCd_{11} (black line); UF_4 (red line); UO_2 (broken blue line). 4(b): UO_2 (black); UF_2 (red); $U(1)F_4$ (green). 4(c) UO_2 (black); UF_4 (red); $U(1)F_4$ (red).
- Figure 5 Shown here are the results of Branching Ratio Calculations using U oxide clusters. The (larger) summed curves are shown in black; the (smaller) representative individual components are shown in various colors. See text for details.
- Figure 6 Comparison of the experimental XAS/XANES measurements of UO_2 and UF_4 (3rd column) with simulated spectra generated with Doniach-Sunjic lineshapes and based upon the cluster calculations of Ryzhkov et al for UO_2 and UF_4 . [50,51] UO_2 (UF_4) curves are shown in black (red). The first column is based solely upon the calculated 6d unoccupied density of states (UDOS) of Ryzhkov et al, using DS lineshapes, where α is the asymmetry parameter and Γ is the half width at half maximum of the Lorentzian part of the DS function. [52] The value of α has been held constant at 0.3, while Γ has been varied systematically. In the middle column, the distribution of UO_2 6d states has been modified to match the UO_2 N_7 XAS spectrum in the third column. The energy of the states has been modified as follows: -2.33 -> -2.33; -5.85 -> -

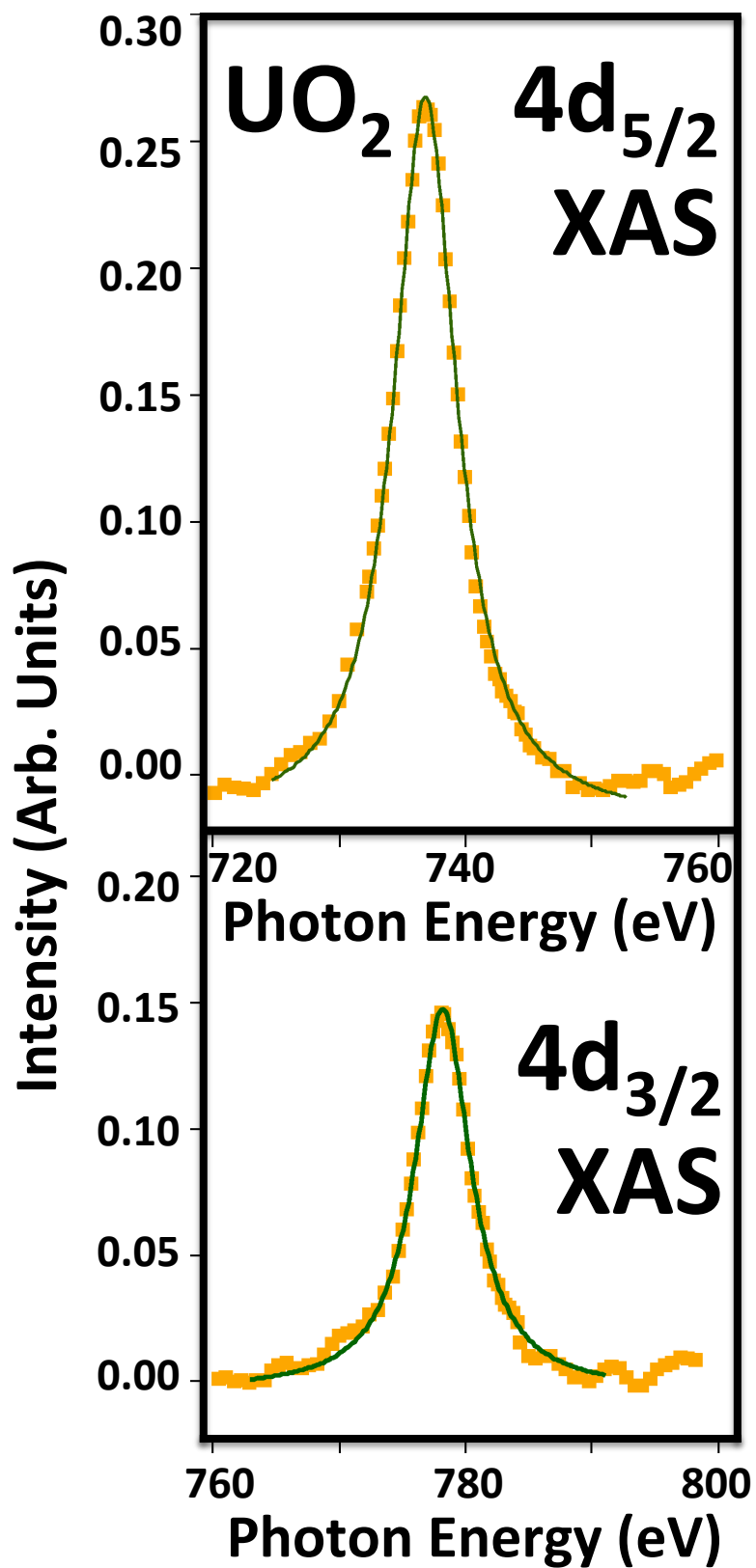
Oxidation and Crystal Field Effects in Uranium

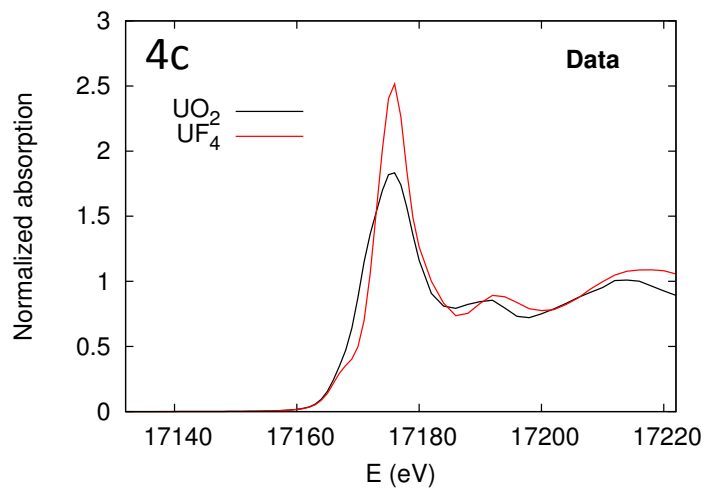
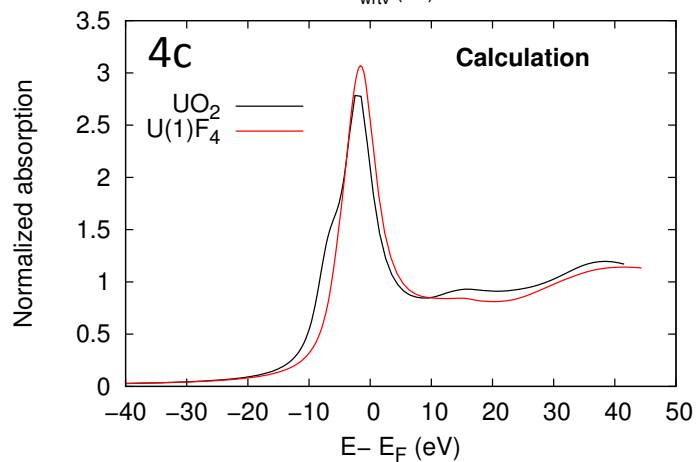
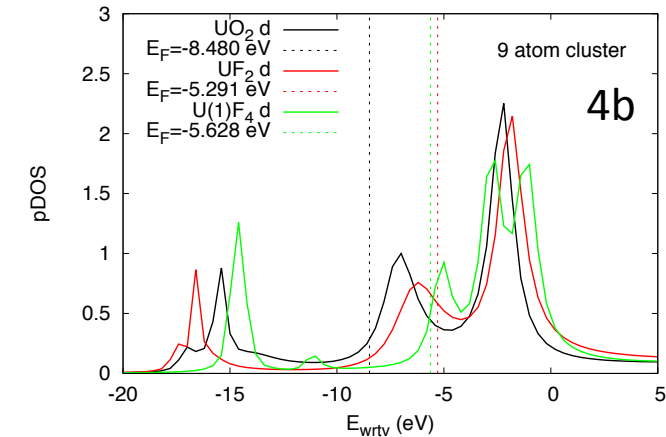
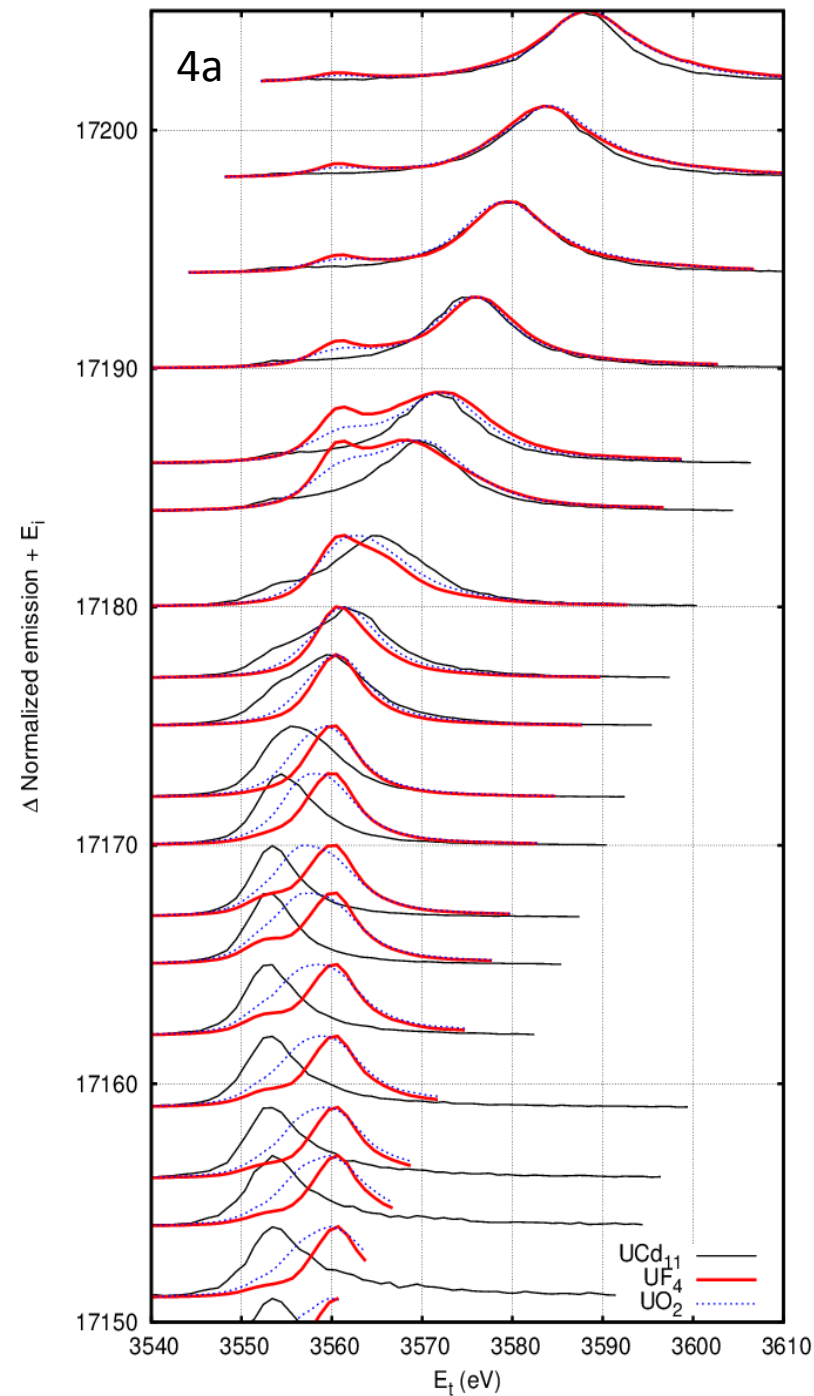
5.85; -6.09 -> -7.85. Thus, only the single highest energy state has been moved. The third column contains the experimental results, for transitions into the 6d UDOS, from the $4f_{7/2}$ (N_7) and $2p_{3/2}$ (L_3) initial states. From UF_4 PFY L_3 edge jump width (width corresponding to 10%-90% intensities), it is found that the FWHM = 3.7, which corresponds to $\Gamma = 1.85$ eV. Thus, for the PFY L_3 spectra, the comparison is made to the $\Gamma = 2$ case. For the "regular" L_3 XANES, the FWHM is on the order of 10 eV, and the comparison is made with the $\Gamma = 4$ eV case. [19]

Figure 7 This figure is a summary of the results for the Branching Ratio of the $4d_{5/2}$ and $4d_{3/2}$ doublet determined from X-ray Absorption Spectroscopy (XAS) and the related technique, Electron Energy Loss Spectroscopy (EELS). The data are also shown in Tables 1 and 2. The jj limit curve is a solid gray line. The solid black line is the intermediate model result, from Table 1. The experimental results, shown typically with error bars of +/- 0.02, are from XAS (filled red diamonds), EELS (hollow blue squares) and UO_2 -STXM and UO_3 -STXM (both- filled orange circle with error bars). There are also new results from cluster calculations for UO_2 and UO_3 (both-filled green circle with error bars). See text for details.

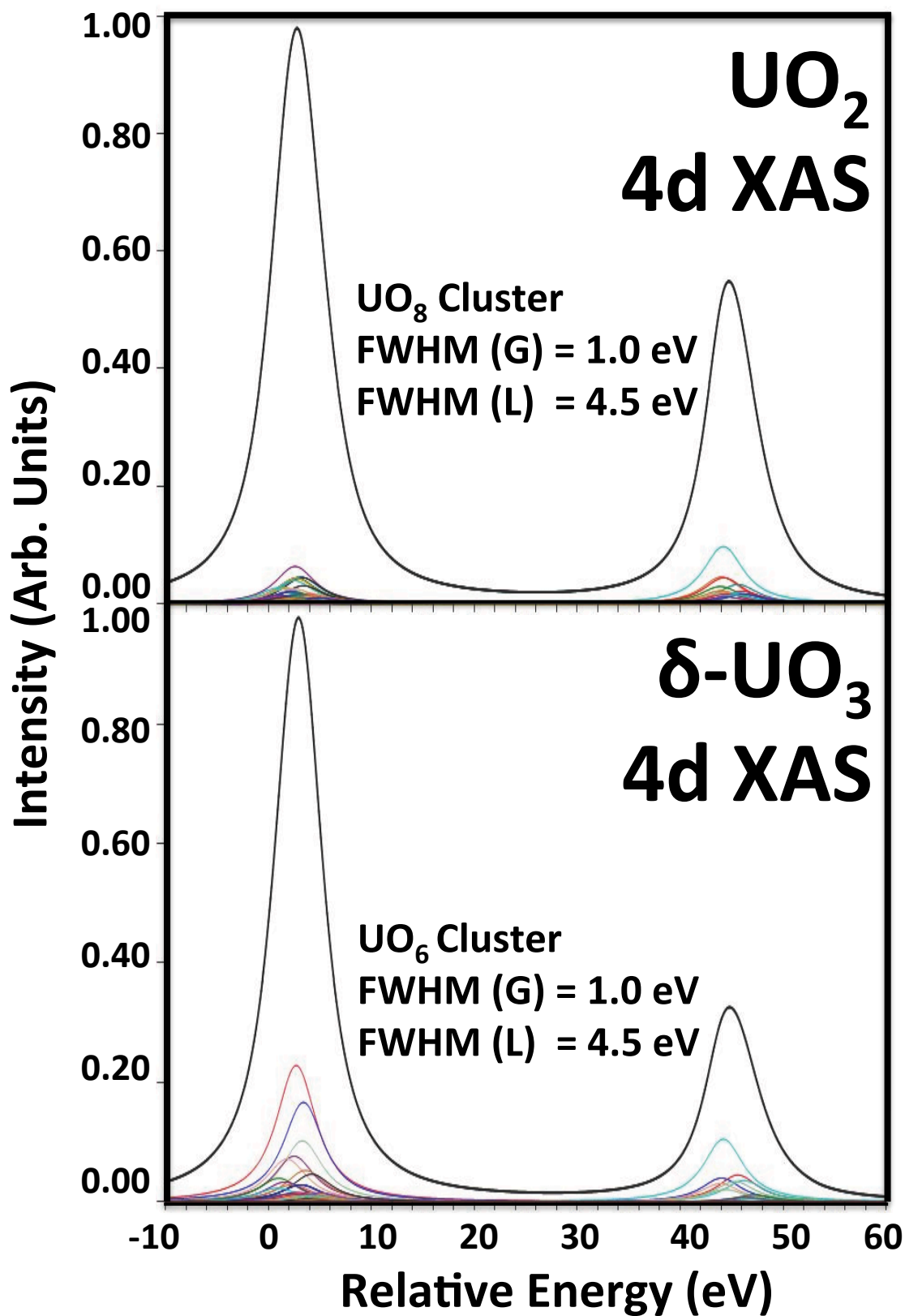








Cluster Calculations



X-Ray Absorption Transitions into the U6d States

Intensity (Arb. Units)

